Photoreceptor discs form through peripherin-dependent suppression of ciliary ectosome release

Raquel Y. Salinas,[1,2]* Jillian N. Pearring,[1]* Jin-Dong Ding,[1]* William J. Spencer,[1,2] Ying Hao,[1] and Vadim Y. Arshavsky[1,2]

[1]Department of Ophthalmology and [2]Department of Pharmacology, Duke University, Durham, NC 27710

The primary cilium is a highly conserved organelle housing specialized molecules responsible for receiving and processing extracellular signals. A recently discovered property shared across many cilia is the ability to release small vesicles called ectosomes, which are used for exchanging protein and genetic material among cells. In this study, we report a novel role for ciliary ectosomes in building the elaborate photoreceptor outer segment filled with hundreds of tightly packed "disc" membranes. We demonstrate that the photoreceptor cilium has an innate ability to release massive amounts of ectosomes. However, this process is suppressed by the disc-specific protein peripherin, which enables retained ectosomes to be morphed into discs. This new function of peripherin is performed independently from its well-established role in maintaining the high curvature of disc edges, and each function is fulfilled by a separate part of peripherin's molecule. Our findings explain how the outer segment structure evolved from the primary cilium to provide photoreceptor cells with vast membrane surfaces for efficient light capture.

Introduction

Our vision begins upon photoexcitation of the visual pigment located in one of many disc membranes stacked inside the ciliary outer segment of rod and cone photoreceptor cells. The functional role of this structural arrangement is well understood. Disc stacks provide vast, layered surfaces for efficient light capture, which is required for the high sensitivity of vertebrate vision (Arshavsky and Burns, 2012). The organization of discs resembles that of chloroplast thylakoids, which likewise evolved to maximize light absorption.

Discs are continuously renewed throughout the lifetime of a vertebrate animal, with older discs being phagocytized by the retinal pigment epithelium (RPE) at the outer segment tip and replaced with new discs formed at the outer segment base (Young, 1967). It is now firmly established that disc formation starts with evagination of the plasma membrane at the outer segment base followed by lateral membrane outgrowth and, in the cases of rods and mammalian cones, subsequent disc enclosure (Kinney and Fisher, 1978; Steinberg et al., 1980; Burgoyne et al., 2015; Ding et al., 2015; Volland et al., 2015). However, the molecular and cellular mechanisms underlying the ongoing disc production remain elusive.

The outer segment is unique among all cilia for its ability to build intraciliary membrane structures. In contrast, many other cilia produce extracellular vesicles called ectosomes (Wood and Rosenbaum, 2015). One proposed function of ectosomes is to perform efficient disposal of select proteins from the cilium, thereby allowing a rapid change in its molecular composition (Nager et al., 2017; Phua et al., 2017). Another perhaps more sophisticated function of ciliary ectosomes is to serve as vehicles for exchanging proteins and genetic material among cells (Hogan et al., 2009; Wood et al., 2013; Wang et al., 2014; Cao et al., 2015; Wood and Rosenbaum, 2015).

We now report that the photoreceptor cilium also has an innate ability to produce massive amounts of ectosomes, but in normal photoreceptors their release is blocked by the protein called peripherin (also known as peripherin-2 and RDS). The ectosomal membranes retained at the cilium through this mechanism are shaped into discs through elongation and flattening to ultimately form the elaborate outer segment structure. This novel function of peripherin is performed by its C-terminal cytoplasmic sequence and does not require the transmembrane core, which is responsible for another, previously established, function of peripherin to provide structural support of highly curved disc rims.

Results

Extracellular vesicles produced by peripherin knockout photoreceptors are ciliary ectosomes

A unique animal model in which photoreceptors produce a primary cilium but do not elaborate it into an outer segment is the

*R.Y. Salinas, J.N. Pearring, and J.-D. Ding contributed equally to this paper.

Correspondence to Vadim Y. Arshavsky: vadim.arshavsky@duke.edu

Abbreviations used: RPE, retinal pigment epithelium; WT, wild type.

The Rockefeller University Press $30.00
J. Cell Biol. Vol. 216 No. 5 1489–1499
https://doi.org/10.1083/jcb.201608081

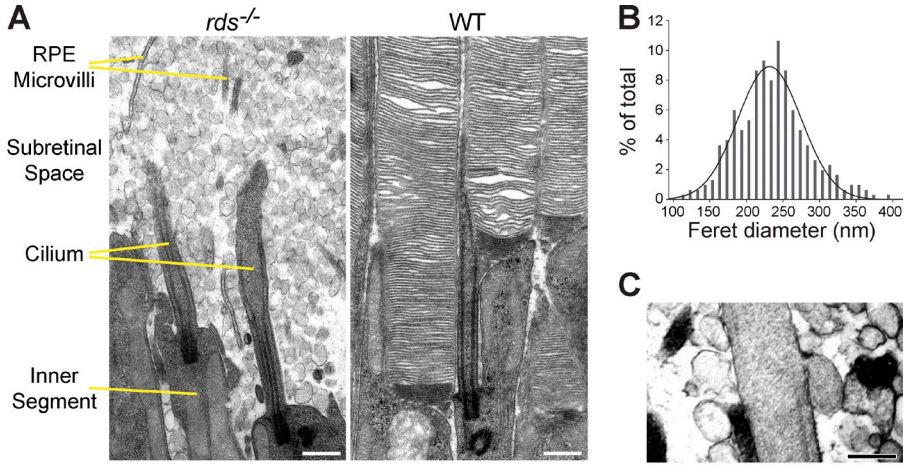

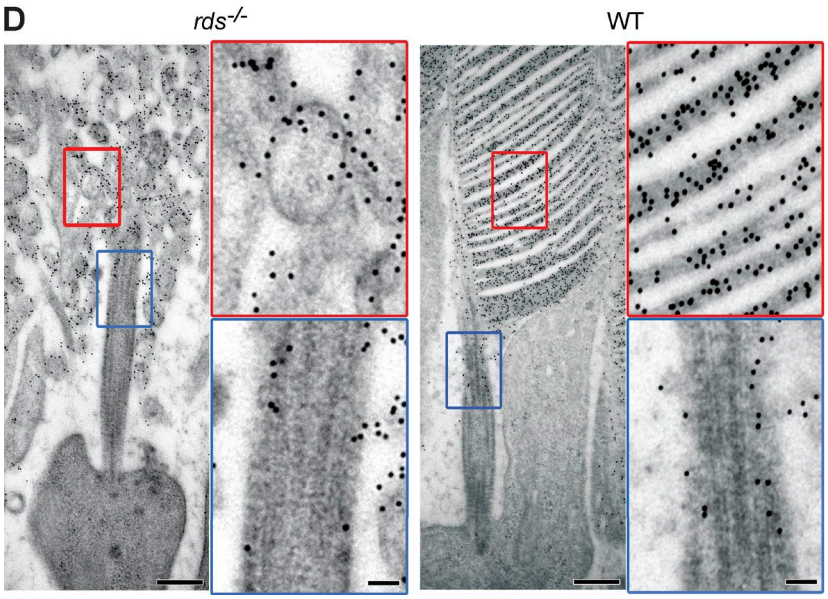

Figure 1. **Ultrastructural analysis of subretinal vesicles in *rds*$^{-/-}$ mice.** (A) EM images of retinal cross sections from *rds*$^{-/-}$ (left) and WT (right) mice at P21. (B) Gaussian histogram of Feret diameters for extracellular vesicles in *rds*$^{-/-}$ retinas (n = 250 pooled from two animals). Means ± SD are shown. (C) An example of extracellular vesicle budding from the ciliary membrane of an *rds*$^{-/-}$ rod. (D) Immunogold labeling of rhodopsin (4D2 mAb) in the distal cilium and extracellular vesicles of a rod photoreceptor in *rds*$^{-/-}$ and WT retina. Insets show magnified areas marked by red and blue rectangles. Bars: (A and D, main images) 500 nm; (C) 200 nm; (D, insets) 100 nm.

peripherin knockout mouse (also known as the *rds*$^{-/-}$ mouse; Sanyal and Jansen, 1981; Travis et al., 1989; Connell et al., 1991). The subretinal space in these mice is filled with vesicular material (Fig. 1 A), which was previously attributed as cellular debris formed because of ongoing photoreceptor degeneration caused by this mutation (Cohen, 1983; Jansen and Sanyal, 1984). However, using a recently developed tissue fixation protocol that enables superior preservation of photoreceptor ultrastructure (Ding et al., 2015), we reexamined *rds*$^{-/-}$ retinas and noticed that the appearance of these vesicles is more in line with ciliary ectosomes than debris. Most of them have similar diameters (231 ± 44 nm; means ± SD; Fig. 1 B), which correspond to typical ectosome dimensions (Cocucci and Meldolesi, 2011), and on occasion, we were able to capture a vesicle still connected to the primary cilium as predicted for a budding ectosome (Fig. 1 C). Consistent with their outer segment origin, these vesicles are highly enriched in rhodopsin (Fig. 1 D; Nir and Papermaster, 1986; Usukura and Bok, 1987).

The hypothesis that subretinal vesicles in *rds*$^{-/-}$ mice are ciliary ectosomes rather than cellular debris predicts that they contain other outer segment proteins but not those from the adjacent cell body. Indeed, immunostaining of an outer segment protein, R9AP, colocalized with rhodopsin immunostaining in extracellular vesicles (Fig. 2 A), as did immunostaining of another outer segment protein, Rom-1 (Fig. 2 B). In contrast, R9AP immunostaining did not overlap with that of Na^+K^+-ATPase present in the photoreceptor plasma membrane (Fig. 2 C).

Another prediction of our hypothesis relates to the orientation of rhodopsin molecules in the membrane of extracellular vesicles formed upon an outward membrane budding event. If these vesicles are ectosomes, rhodopsin's C terminus should be located inside the lumen, whereas its N terminus is exposed outside. This is in contrast to discs, whose enclosure results in rhodopsin assuming an opposite membrane orientation with its N and C termini exposed at the luminal and cytoplasmic disc surfaces, respectively. We immunostained retinal cross sections of *rds*$^{-/-}$ mice with antibodies recognizing either the N or C terminus of rhodopsin (4D2 and 1D4, respectively; Fig. 2 D). Although both antibodies labeled rhodopsin in sections permeabilized with detergent, only the N-terminal antibody labeled sections that were not permeabilized. Therefore, these vesicles expose rhodopsin's N terminus outside, as predicted for ectosomes but not for discs.

We next examined postembryonic development of the *rds*$^{-/-}$ rod cilium to capture when and where the first vesicles are formed (Fig. 3). The biogenesis of primary cilia, including the outer segment, begins with an attachment of a ciliary vesicle to the basal body followed by axoneme extension with simulta-

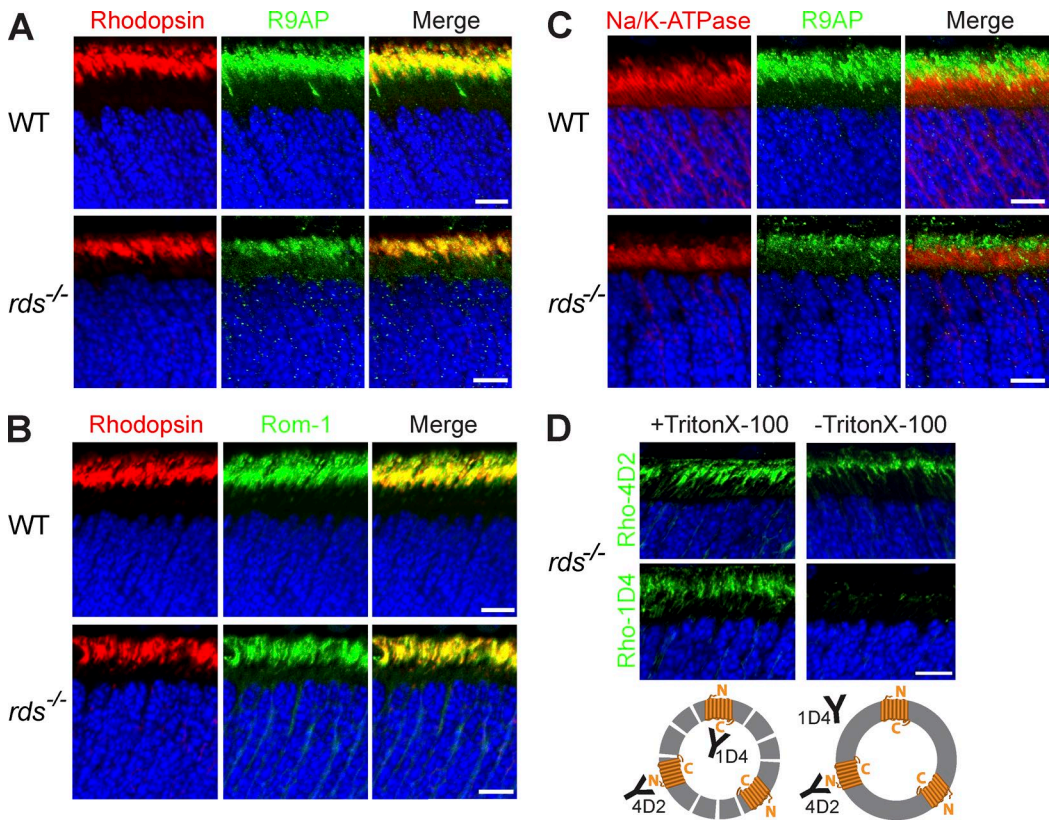

Figure 2. **Subretinal vesicles in *rds*$^{-/-}$ mice are ciliary ectosomes.** (A and B) Immunostaining of rhodopsin (1D4) with the outer segment proteins R9AP (A) and Rom-1 (B) in cross sections of WT and *rds*$^{-/-}$ retinas. (C) Immunostaining of Na^+K^+-ATPase and R9AP in cross sections of WT and *rds*$^{-/-}$ retinas. (D) Rhodopsin immunostaining with N-terminal (4D2) and C-terminal (1D4) antibodies in *rds*$^{-/-}$ retinal cross sections with and without Triton X-100 treatment. Below is a cartoon representation of extracellular vesicles and antibodies under each condition. In all panels, mice are at P14 and nuclei are stained with Hoechst (blue). Bars, 10 µm.

neous vesicle expansion, ciliary vesicle fusion with the plasma membrane, and additional axoneme elongation to form the cilium (Sorokin, 1962; Sedmak and Wolfrum, 2011; Pearring et al., 2013). These early ciliogenesis steps proceed identically in wild-type (WT) and *rds*$^{-/-}$ rods. However, around postnatal day (P) 10, when WT rods produce their first discs, *rds*$^{-/-}$ rods start releasing vesicles at the distal ends of their cilia. After this developmental stage, WT rods continued to build and elongate their outer segment structure, whereas cilia in *rds*$^{-/-}$ mice remained at the same length (~3 µm; Fig. S1) and continued to release vesicles into the surrounding space. Collectively, these data demonstrate that extracellular vesicles produced by *rds*$^{-/-}$ photoreceptors meet all criteria of being ciliary ectosomes.

Ectosomes are occasionally produced by the primary cilia of developing photoreceptor cells

Remarkably, the ability to produce ectosomes could also be documented for WT photoreceptors during a narrow window of their postnatal development. Thorough examination of ultrastructural images from WT retinas collected at P10 revealed that ~3% of rods produce rhodopsin-positive vesicles at their ciliary tips, whose appearance is identical to ectosomes in *rds*$^{-/-}$ mice (Fig. 4, A and B). This suggests that at the onset of disc morphogenesis, a small population of rods may experience a delay in peripherin expression, resulting in the release of a few ectosomes before discs are formed. Consistently, ectosomes were never observed in WT retinas at P14 or later, indicating that any such mismatch is settled by this age and that the few ectosomes produced earlier are likely cleared by the RPE.

The idea of a potential mismatch between photoreceptor development and peripherin expression in a subset of photoreceptors was further supported by examining ectosome production in P10 *rds*$^{+/-}$ mice characterized by reduced peripherin expression (Nour et al., 2004). In this case, the prevalence of photoreceptors producing clusters of ectosomes at P10 increased from 3% to 12.8% (Fig. 4, C and D).

The ability of peripherin to suppress ectosomal release is confined to its intracellular C terminus

The data obtained so far indicate that peripherin is a molecule responsible for preventing ectosome release from photoreceptors. This provides their cilia with membrane material required to build discs. A well-established function of peripherin is to induce membrane bending and support the highly curved structure of disc edges (Stuck et al., 2016). In the remaining experiments, we demonstrate that peripherin's functions to arrest ectosome release and to bend membranes are not mutually dependent and are confined to different parts of the peripherin molecule: the cytoplasmic C terminus and tetraspanin membrane core, respectively.

Two recombinant constructs representing each part of the peripherin molecule, along with a full-length peripherin control, were expressed in rods using the technique of in vivo electroporation (Matsuda and Cepko, 2004). In the first construct, the C

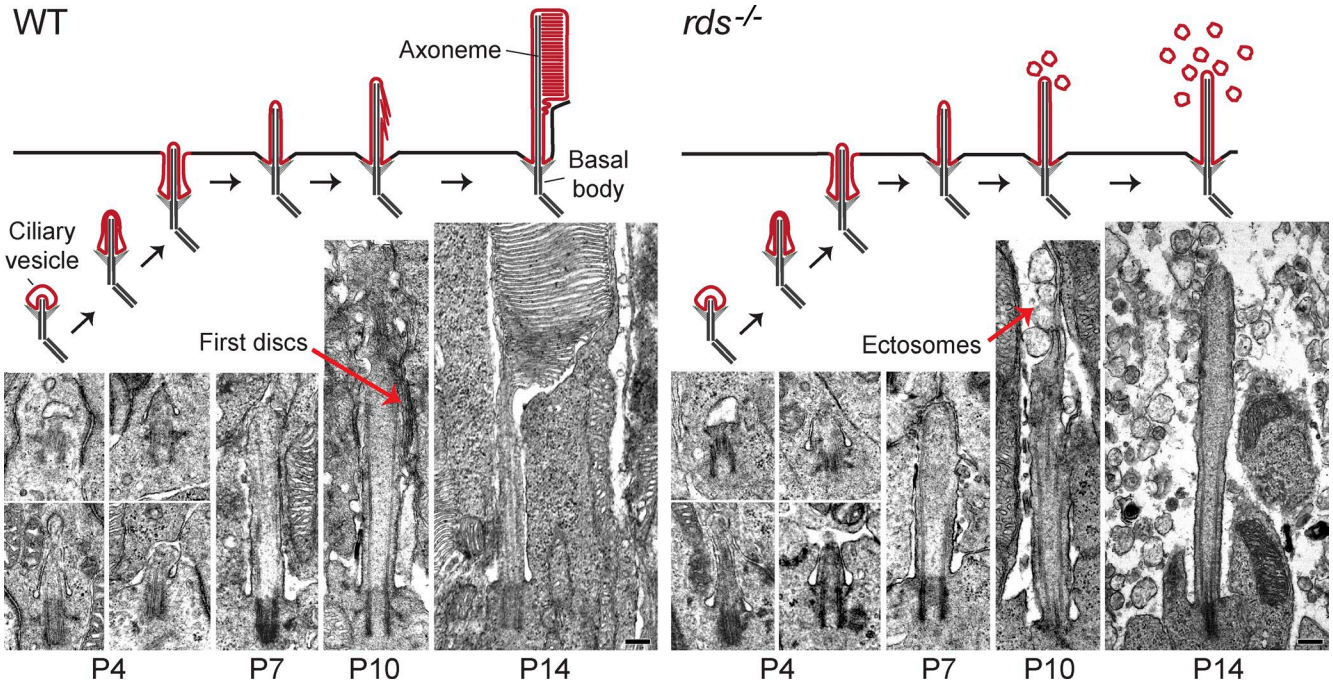

Figure 3. **Developmental stages of the photoreceptor cilium in WT and *rds*$^{-/-}$ mice.** EM images showing the progression of rod outer segment morphogenesis at the indicated postnatal ages for WT and *rds*$^{-/-}$ retinas. At P10, red arrows highlight the first discs that form at the end of the cilium in WT rods, as opposed to ectosomes that form in *rds*$^{-/-}$ rods. Schematic representations of each developmental stage are shown above their corresponding images. Bars, 200 nm.

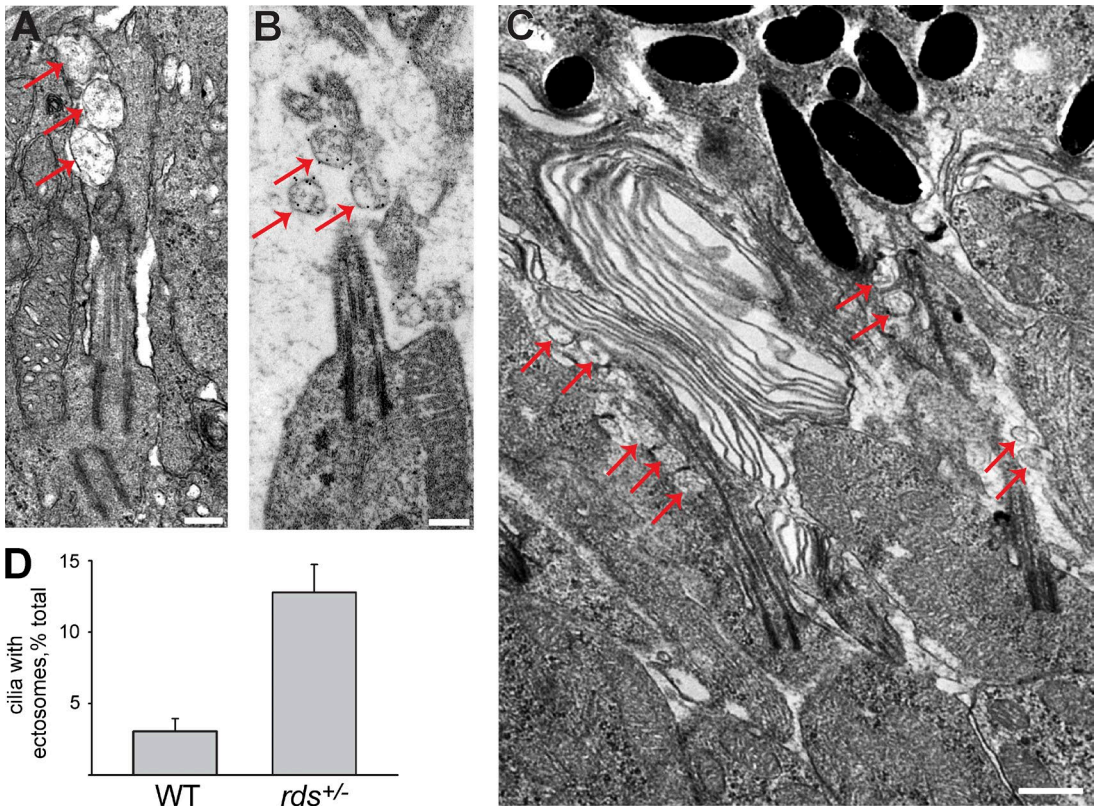

Figure 4. **Ectosome occurrence in 10-d-old WT and *rds*$^{+/-}$ mice.** (A) EM image of a WT rod with ectosomes next to the distal ciliary end. (B) Immunogold labeling of rhodopsin (4D2 mAb) in these ectosomes. (C) EM image of an *rds*$^{+/-}$ retina with three ectosome clusters next to developing cilia. Red arrows point to ectosomes. Bars: (A and B) 200 nm; (C) 500 nm. (D) The prevalence of cilia with adjacent ectosomes in WT and *rds*$^{+/-}$ retinas. Between 350 and 450 cilia were analyzed in three retinas of each genotype. Data are averaged among three retinas and shown as SEM.

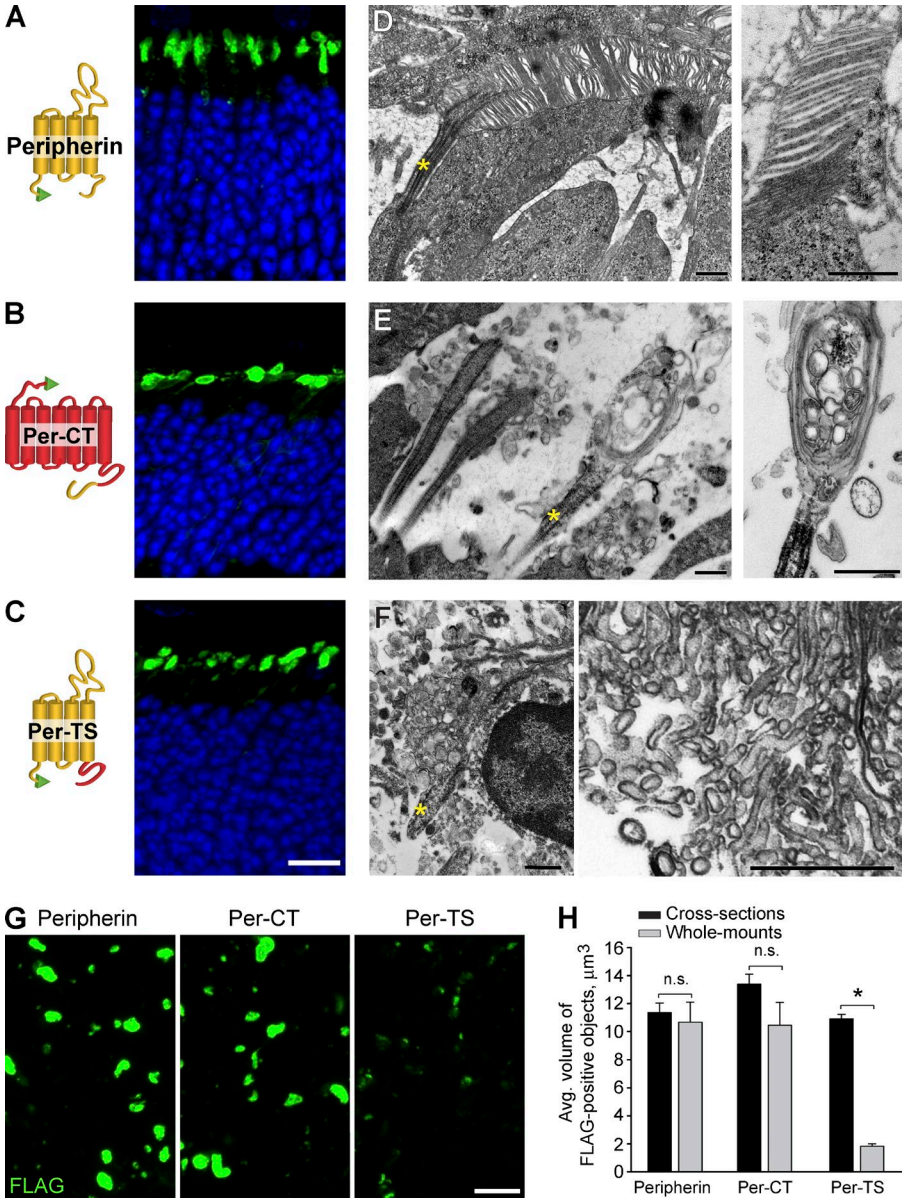

Figure 5. **Transfection of FLAG-tagged recombinant peripherin constructs into rods of *rds*$^{-/-}$ mice.** (A–C) FLAG immunostaining in cross sections of retinas transfected with peripherin (A), Per-CT (B), and Per-TS constructs (C). A cartoon representation of each construct is shown on the left side of each corresponding panel with peripherin sequences shown in yellow, rhodopsin sequences shown in red, and the FLAG tag shown in green. Nuclei are stained with Hoechst (blue). (D–F) EM images of cilia from rods transfected by peripherin (D), Per-CT (E), and Per-TS (F) constructs. Yellow asterisks mark cilia. (G) FLAG immunostaining of retinal wholemounts transfected by each construct after RPE detachment. Bars: (A–C and G) 10 µm; (D–F) 500 nm. (H) Mean volumes of FLAG-positive objects for each construct in retinal cross sections and wholemounts. The data are averaged from at least six individual retinas of each type and are shown as SEM. *, P = 0.009; n.s., not significant. Student's *t* test.

terminus of peripherin was fused behind full-length rhodopsin to achieve membrane attachment and expose it to the cytosolic side of the ciliary membrane (Per-CT construct; Fig. 5). We expected this construct to be targeted to the outer segment because both rhodopsin and peripherin's C termini contain outer segment targeting motifs (Tam et al., 2000, 2004; Salinas et al., 2013). The second construct contained peripherin's tetraspanin core fused to rhodopsin's C terminus (Per-TS construct; Fig. 5), with the latter providing an outer segment targeting signal (Tam et al., 2000). An N-terminal FLAG tag was added to each construct for easy detection.

We first confirmed that each construct was reliably expressed in the outer segments of WT rods and that their expression was comparable to that of FLAG-tagged rhodopsin (note that only a subset of rods was typically transfected by this technique; Fig. S2). We next expressed these constructs in *rds*$^{-/-}$ rods and found each to be localized in structures of comparable sizes and shapes atop the photoreceptor cell layer (Fig. 5, A–C).

Despite the similar localization and sizes of these structures, their appearance in EM images was strikingly different. As expected, full-length peripherin restored normal-looking outer segments containing disc stacks inside (Fig. 5 D). *Rds*$^{-/-}$ rods expressing Per-CT also produced ciliary extensions, but instead of discs, they contained vesicular material surrounded by multiple membrane layers (Fig. 5 E; this phenotype is contrasted by the two neighboring cells on the left that display an *rds*$^{-/-}$ nontransfected phenotype). This indicates that peripherin's C terminus is sufficient for outer segment membrane retention, but the structural organization of the resulting outer segment is severely distorted without peripherin's core supporting the subsequent stages of disc morphogenesis. Unfortunately, our attempts to further narrow the region within peripherin's C terminus responsible for ciliary membrane retention were unfruitful because of an unforeseen property of these constructs (designed similar to Per-CT but with shortened C-terminal sequences) to get stuck in biosynthetic membranes of transfected rods (not depicted).

The expression of Per-TS produced a different type of unusual structure consisting of tightly packed clusters of membrane vesicles, often tubular in shape (Fig. 5 F). These clus-

ters were typically intertwined with RPE microvilli and did not appear to be attached to the photoreceptor cilium. These membrane clusters displayed strong immunogold staining with an anti-FLAG antibody, consistent with their origin from electroporated rods (Fig. S3).

To further demonstrate that membrane structures produced upon expression of Per-CT are connected to the photoreceptor cilium, whereas those produced upon expression of Per-TS are not, we immersed freshly dissected eyecups into Ringer's solution and gently separated retinas from the RPE. The resulting detached retinal wholemounts were stained with an anti-FLAG antibody (Fig. 5 G). Consistent with EM observations, the surfaces of retinas expressing Per-CT and control peripherin retained FLAG-positive structures of size and shape similar to those in retinal cross sections (Fig. 5, A–C). In contrast, the surfaces of retinas expressing Per-TS contained much smaller FLAG-positive puncta, likely ciliary tips, indicating that the membrane clusters were not connected to the cilium and were lost upon retinal detachment. Quantitative analysis showed that the mean volumes of FLAG-positive structures in retinal cross sections and isolated wholemounts were essentially identical for Per-CT and peripherin, whereas the mean volume of Per-TS–induced structures was reduced by more than fivefold upon retinal detachment (Fig. 5 H).

As expected, FLAG-positive structures produced upon Per-CT and peripherin expression were costained with an antibody against the outer segment marker, Rom-1 (Fig. S4). Rom-1 immunostaining outside these structures was punctate, likely representing ciliary tips of nontransfected cells. Consistently, only punctate Rom-1 staining was observed in wholemounts expressing Per-TS (Fig. S4).

To confirm that the ciliary membrane retention observed upon Per-CT expression in *rds*$^{-/-}$ rods was not caused by the rhodopsin part of this construct, we expressed full-length FLAG-tagged rhodopsin (i.e., Per-CT construct lacking peripherin's C terminus). Unlike the constructs in Fig. 5, FLAG immunostaining of retinal cross sections displayed a punctate pattern in the subretinal space, and only small FLAG-positive puncta were detected upon retinal detachment from the RPE (Fig. 6, A and B). These observations are consistent with FLAG-tagged rhodopsin being released in ectosomes produced by transfected cells.

Finally, we tested whether ciliary membrane retention by peripherin's C terminus could be preserved if rhodopsin were replaced with an alternative ciliary membrane carrier. *Rds*$^{-/-}$ rods were electroporated with constructs in which peripherin's C terminus was cloned behind FLAG-tagged serotonin-6 (Htr-6) or somatostatin-3 (Sstr-3) receptors. Although neither receptor is naturally expressed in rods, they contain strong ciliary targeting signals (Händel et al., 1999; Pearring et al., 2015; Geneva et al., 2017). As observed with Per-CT, *rds*$^{-/-}$ rods electroporated with either construct produced ciliary extensions that were retained upon retinal detachment (Fig. S5). The only difference is that their volume was approximately half of the extensions produced by Per-CT, likely reflecting a lower expression efficiency of these receptors in rods than in rhodopsin.

The ability of peripherin to induce membrane curvature is confined to its tetraspanin domain

We noted that the tubular shape of extracellular vesicles produced upon Per-TS expression (Fig. 5 F) resembles that of liposomes reconstituted with full-length peripherin in vitro (Kevany et al., 2013) as well as intracellular membranes produced upon peripherin expression in cell culture (Khattree et al., 2013). This suggests that peripherin's core is sufficient to support this type of membrane bending. To test this directly, we expressed all three peripherin constructs in cell culture according to the strategy outlined by Khattree et al. (2013) and observed production of numerous intracellular tubular membranes upon expression of both core-containing constructs, peripherin and Per-TS (Fig. 7, A and B). None of these membrane structures were observed upon expression of Per-CT (Fig. 7 C).

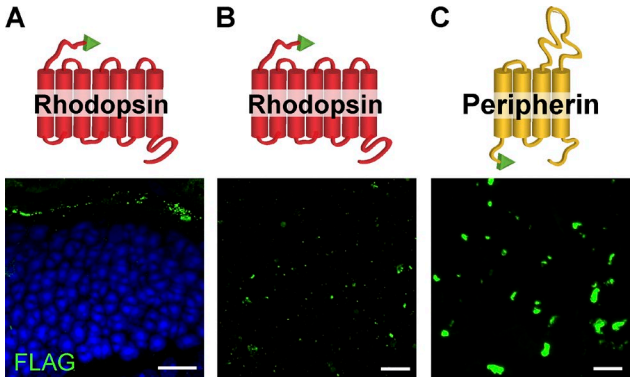

Figure 6. **Transfection of FLAG-tagged rhodopsin into rods of *rds*$^{-/-}$ mice.** (A) FLAG immunostaining in a retinal cross section. (B) FLAG immunostaining in a detached retinal wholemount. (C) FLAG immunostaining in a wholemount retina transfected with FLAG-tagged peripherin for comparison. A cartoon representation of each construct is shown above its corresponding panel. Bars, 10 µm.

Immunohistochemical analysis showed that the bulk of full-length peripherin did not colocalize with markers representing the endoplasmic reticulum, Golgi, or plasma membrane, and the same was true for Per-TS (Fig. 7, A and B). This is consistent with conclusions by Khattree et al. (2013) that peripherin exiting biosynthetic membranes of cultured cells accumulates in intracellular vesicles uniquely shaped by its presence. In contrast, a large portion of Per-CT colocalized with both the endoplasmic reticulum and the plasma membrane. The latter suggests that a significant amount of this construct exits biosynthetic membranes but does not cause any membrane bending en route to its final plasma membrane destination, as seen in the corresponding EM images in Fig. 7 C. These data demonstrate that the tetraspanin core of peripherin is responsible for membrane bending and does not require peripherin's C terminus to perform this function.

Discussion

The mechanism of photoreceptor outer segment morphogenesis has remained among the most puzzling problems in vision since discs were discovered over 60 years ago (Sjöstrand, 1953). Our study provides a conceptual breakthrough in understanding how the elaborate outer segment structure develops from the primary cilium. We demonstrate that the photoreceptor cilium may exist in two distinct functional states: it either releases massive amounts of ectosomes or retains and morphologically transforms them into discs (Fig. 8). Remarkably, the entire transition between these states is regulated by peripherin, a protein long known to perform a completely different function of supporting the highly curved structure of mature disc edges (Molday et al.,

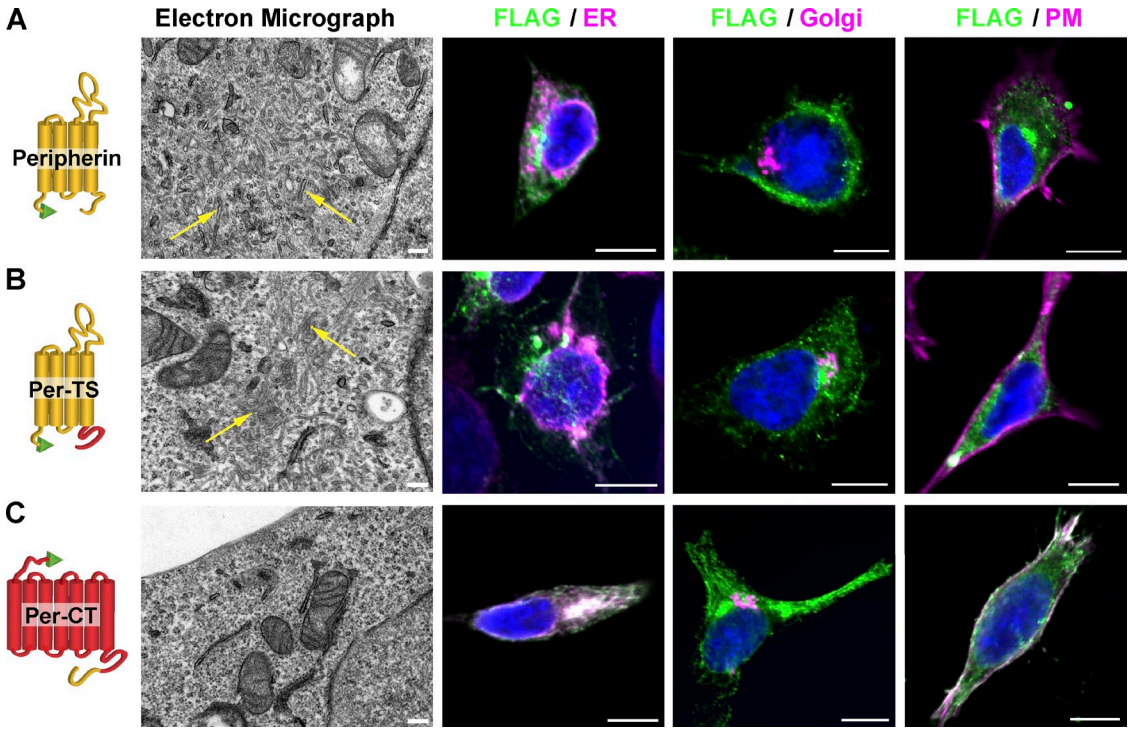

Figure 7. **The tetraspanin core of peripherin is involved in forming highly curved membrane shapes.** (A–C) AD293 cells were transfected with either full-length FLAG-tagged peripherin (A), Per-TS (B), or Per-CT (C). Left panels show representative EM images illustrating the accumulation of intracellular tubular membranes in cells transfected with peripherin or Per-TS (representative examples of tubular membranes are marked with yellow arrows) but not in cells transfected with Per-CT. Right panels show immunostaining of each construct probed with anti-FLAG antibodies (green) in relation to markers of the endoplasmic reticulum (calnexin), Golgi (GM130), and plasma membrane (PM; Na^+K^+-ATPase). All markers are shown in magenta. Nuclei are stained with Hoechst (blue). Bars: (left) 200 nm; (right) 10 µm.

1987; Kevany et al., 2013; Khattree et al., 2013; Goldberg et al., 2016; Stuck et al., 2016).

Distinct peripherin functions are performed by distinct structural elements

We further demonstrate that peripherin's ability to retain ectosomes at the outer segment cilium and its function of supporting membrane edges are fulfilled by different structural elements. The suppression of ectosome release is performed by the C terminus, whose expression in rods is sufficient for retaining membranes at their ciliary tips. However, the resulting ciliary extensions have abnormal structure, containing both layered and vesiculated membranes inside. This highlights the significance of peripherin's tetraspanin core for maintaining the highly organized structure of disc stacks.

The C terminus of peripherin is not homologous to other proteins. Its most prominent structural feature is the amphipathic helix spanning across residues 310–328, which was demonstrated to promote membrane fusion in vitro (Boesze-Battaglia and Goldberg, 2002). It was suggested that this property may be relevant to the process of disc enclosure. However, as recently pointed out by Goldberg et al. (2016), disc enclosure is initiated at the membrane surface opposite to where peripherin's C terminus is exposed, which leaves the functional significance of this fusogenic activity enigmatic. The C terminus is also responsible for peripherin's outer segment targeting (Tam et al., 2004), a function confined to a highly conserved ∼10–amino acid sequence (residues 327–336), including an indispensable valine at position 332 (Salinas et al., 2013).

Another study reported that a synthetic peptide corresponding to peripherin's C terminus induces membrane bending in vitro upon reconstitution with liposomes (Khattree et al., 2013), leading the authors to suggest that the C terminus is responsible for supporting the curvature of disc edges. However, this conclusion contradicts the structural model in which the primary role of supporting this curvature belongs to peripherin's tetraspanin core (Kevany et al., 2013). Our data are also consistent with the tetraspanin core, but not the C terminus, being responsible for this function. We demonstrate that expression of the tetraspanin core construct in both rods and cultured cells causes the formation of highly curved membrane structures. This is not observed upon expression of the construct containing peripherin's C terminus, which suggests that the original observation with the synthetic peptide was likely an epiphenomenon of in vitro reconstitution.

Disc morphogenesis: What remains to be explained

The descriptive understanding of disc morphogenesis has undergone an interesting evolution. The earliest studies postulated that discs are formed upon serial membrane evaginations at the outer segment base (Kinney and Fisher, 1978; Steinberg et al., 1980). This concept was later challenged by suggesting that, at least in mammalian rods, discs are formed through vesicular fusion at the same location (Chuang et al., 2007). However, three recently published papers used an array of modern ultrastructural techniques to prove that discs are formed through the membrane evagination mechanism and explained how tissue fixation artifacts can lead to membrane vesiculation at the outer segment base (Burgoyne et al., 2015; Ding et al., 2015; Volland

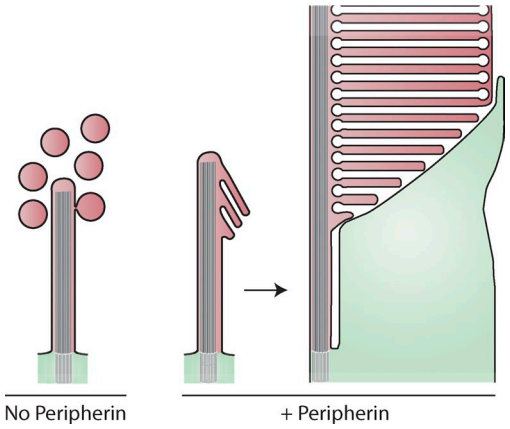

Figure 8. **Schematic illustration of photoreceptor cilium development with and without peripherin.** Shaded red and green areas are topologically equivalent and represent cytoplasmic space in photoreceptor outer and inner segments, respectively. Extracellular space and disc lumens are white.

et al., 2015). The mechanistic insight obtained in our study is perfectly aligned with this overall concept of evagination: a new disc is born as an ectosome whose release is prevented by peripherin. The challenge of future studies is to identify the molecular components of ectosome-releasing machinery in photoreceptors and pinpoint the specific mechanism of peripherin action. Conversely, it will be interesting to investigate whether peripherin's C terminus could affect ciliary ectosome release in other cells.

Clearly, the suppression of ectosome release is just the first of several steps in disc formation. Other steps include disc flattening, elongation, and, in rods and most mammalian cones, enclosure of a disc once its final diameter is reached. In addition to peripherin, there are only a few hints regarding participating molecular components. One of them is prominin-1, also found in microvilli and primary cilia tips, where it is implicated in the stabilization of curved membrane protrusions (Huttner and Zimmerberg, 2001; Iglič et al., 2006). Prominin-1 is expressed at the growing disc edges, and its knockout causes misalignment of discs and eventual photoreceptor degeneration (Yang et al., 2008; Zacchigna et al., 2009; Han et al., 2012).

Another potential player in the process of disc maturation is protocadherin-21, a prominin-1 binding partner (Yang et al., 2008) with a similar localization pattern (Rattner et al., 2001, 2004). The knockout of protocadherin-21 also results in disc misalignment and photoreceptor death (Rattner et al., 2001). More recently, ultrastructural analysis suggested that protocadherin-21 located at the leading edges of newly formed discs makes junctions with the inner segment plasma membrane (Burgoyne et al., 2015), which may regulate the process of disc elongation. Understanding how these proteins work as a coordinated ensemble and identifying the missing components are the challenges for future studies.

In conclusion, our findings provide a striking example of how a single multifunctional protein plays a vital role in transforming a ubiquitous and conserved organelle, the primary cilium, into a highly specialized sensory organelle with unique anatomical organization. One can further speculate that peripherin-dependent arrest of ectosomal release was the pivotal evolutionary event that enabled highly sensitive vertebrate vision as we know it today.

Materials and methods

Animals

Mice were handled according to the protocols approved by the Institutional Animal Care and Use Committees of Duke University (registry numbers A212-12-08 and A011-14-01). Albino WT CD1 mice used in electroporation experiments were obtained from Charles River; pigmented WT C57BL/6J mice and *rds*$^{-/-}$ mice used for immunofluorescence, Western blotting, and EM were obtained from The Jackson Laboratory. The *rds*$^{-/-}$ mouse was described by Sanyal and Jansen (1981) and was subsequently shown to be a peripherin-null allele by Ma et al. (1995). All mice were housed under a 12/12-h light cycle. The experimenters were not blinded to genotype or treatment conditions.

Antibodies

Rabbit polyclonal anti-peripherin antibody was described by Kedzierski et al. (1999), rabbit polyclonal anti-R9AP antibody was described by Keresztes et al. (2004), and sheep polyclonal anti–Rom-1 antibody was generated in our laboratory (Gospe et al., 2010). The following commercial antibodies were used: mouse monoclonal 1D4 against the rhodopsin C terminus (ab5417; Abcam), mouse monoclonal 4D2 against the rhodopsin N terminus (ab98887; Abcam), mouse monoclonal anti–Na^+/K^+-ATPase (sc-58628; Santa Cruz Biotechnology, Inc.), mouse monoclonal anti-FLAG M2 (F1804; Sigma-Aldrich), rabbit polyclonal anti-FLAG (F7425; Sigma-Aldrich), mouse monoclonal anti-GM130 (610822; BD), and rabbit polyclonal anticalnexin (Sigma-Aldrich; C4731).

DNA constructs

DNA constructs were generated using standard PCR-based subcloning methods. Mouse peripherin and rhodopsin fusion constructs were generated by overhang extension PCR. Peripherin was split at amino acid 290. The Per-TS construct contained the first 1–290 amino acids of peripherin fused to rhodopsin's C terminus, amino acids 310–349. The Per-CT construct contained full-length rhodopsin fused to peripherin's C terminus, amino acids 291–346. The FLAG tag was appended to full-length rhodopsin or peripherin's N terminus by introducing its sequence into the forward primer. For the Htr6-CT and Sstr3-CT constructs, a 3×FLAG tag followed by peripherin's C terminus was fused to the C terminus of full-length Htr6 or Sstr3. All forward and reverse primers were designed to introduce 5′-AgeI and 3′-NotI sites, respectively. The following primers were used: for peripherin, 5′-GATCCACCGGTATGGACTACAAGGACGACGACGACAAGGCGCTGCTCAAAGTCAAGTTTG-3′ and 5′-AAGATGCGGCCGCTCAGCCAGCCTCTGGAGCCGGGCCTGC-3′. For rhodopsin, 5′-GCATCCACCGGTATGGATTACAAGGATGACGACGATAAGAACGGCACAGAGGGCCC-3′ and 5′-AAGATGCGGCCGCTCAGGCTGGAGCCACCTGGCTGGTCTCC-3′. For Per-CT, 5′-GCATCCACCGGTATGGATTACAAGGATGACGACGATAAGAACGGCACAGAGGGCCC-3′, 5′-CAGTTCCGGAACTGCTTGTTCAGCGCTGTGTGGAGGTAGCG-3′, 5′-CGCTACCTCCACACAGCGCTGAACAAGCAGTTCCGGAACTG-3′, and 5′-AAGATGCGGCCGCTCAGCCAGCCTCTGGAGCCGGGCCTGC-3′. For Per-TS, 5′-GATCCACCGGTATGGACTACAAGGACGACGACGACAAGGCGCTGCTCAAAGTCAAGTTTG-3′, 5′-CAGTTCCGGAACTGCTTGTTCAGCGCTGTGTGGAGGTAGCG-3′, 5′-CGCTACCTCCACACAGCGCTGAACAAGCAGTTCCGGAACTG-3′, and 5′-AAGATGCGGCCGCTCAGGCTGGAGCCACCTGGCTGGTCTCC-3′. For Htr6-CT, 5′-TAAGTACCGGTGCCACCATGGTTCCAGAGCCCGGCCCT-3′, 5′-CACTTGGTTCCCCCATGAACGACTACAAAGACCATGACGGT-3′, 5′-ACCGTCATGGTCTTTGTAGTCGTTCATGGGGGAACCAAGTG-3′, and 5′-TACTTAGCGGCCGCCTAGCCAGCCTCTGGAGCC-3′. For Sstr3-CT, 5′-TAAGTACCGGTGCCA

CCATGGCCACTGTTACCTATCCT-3′ and 5′-TACTTAGCGGCC GCCTAGCCAGCCTCTGGAGCC-3′.

For in vivo electroporation constructs, PCR products were subcloned into the pRho plasmid, driving gene expression under the 2.2-kb bovine rhodopsin promoter (plasmid 11156; Addgene). For cell culture constructs, PCR products were subcloned into the pEGFPN-1 plasmid, driving gene expression under the CMV promoter (6085-1; Takara Bio Inc.). All constructs were confirmed by direct sequencing.

In vivo electroporation of mouse retinas

Retinal transfection of neonatal mice by the in vivo electroporation technique (Matsuda and Cepko, 2007) was used with modifications described by Pearring et al. (2014, 2015) to express exogenous constructs in mouse rods. After anesthetization of neonatal mice (P1) on ice, the eyelid and sclera were punctured at the periphery of the eye using a 30-gauge needle. A blunt-end 32-gauge needle was advanced through the puncture wound until it reached the subretinal space, and 0.3–0.5 µl of concentrated plasmid DNA (4 µg/µl of the construct of interest and 2 µg/µl mCherry to visualize transfected cells) was deposited. A tweezer-type electrode (BTX) was placed over the mouse's head with the positive electrode overlying the injected eye. Five 100–110-V pulses of 50-ms duration were applied using a square pulse generator (ECM830; BTX). Neonates were returned to their mother and allowed to develop until P21, when mice were sacrificed by CO_2 inhalation followed by decapitation. A minimum of 20 positively expressing retinas were analyzed for each DNA construct in different assays.

Immunofluorescence

Experiments were performed essentially as previously described (Salinas et al., 2013; Pearring et al., 2014, 2015) as follows. For retinal cross sections, mouse posterior eyecups were fixed for 1 h in 4% paraformaldehyde in mouse Ringer's solution, rinsed three times in PBS, and embedded in 7.0% low-melt agarose (A3038; Sigma-Aldrich). 100-µm cross sections through the central retina were collected using a vibratome (VT1200S; Leica Biosystems), placed in 24-well plates, and blocked in 5% goat serum and 0.5% Triton X-100 in PBS for 1 h at 22°C. Sections were incubated in primary antibody diluted in blocking solution overnight at 4°C, rinsed three times, and incubated with 10 µg/ml Hoechst 33342 (H3569; Thermo Fisher Scientific) and goat or donkey secondary antibodies conjugated with Alexa Fluor 488, 568, or 647 (Invitrogen) in blocking solution for 2 h at 22°C. Sections were mounted with Fluoromount (Electron Microscopy Sciences) and coverslipped. For retinal wholemounts, posterior eyecups from electroporated mice were microdissected to obtain mCherry-positive patches using a fluorescent microscope (M165FC; Leica Microsystems) equipped with a Plan Apochromat 1.0× objective and an ET RFP filter (Leica). The retinal patch was then placed with the RPE side up on a nitrocellulose membrane. Using forceps, the RPE was gently removed from the retina patch. Each patch was submerged three times in PBS before being fixed for 1 h with 4% paraformaldehyde in mouse Ringer's solution, rinsed three times in PBS, and placed in a 24-well plate. Retinal patches were then immunostained as described above for retinal cross sections. Images were acquired using a microscope (Eclipse 90i; Nikon) equipped with a 60× oil immersion objective (1.40 NA; Plan Apochromat VC) and an A1 confocal scanner controlled by NIS-Elements Advanced Research software (Nikon) for image acquisition. Manipulation of images was limited to adjusting the brightness level, image size, and cropping using either NIS-Elements Advanced Research software or Photoshop (Adobe). Volumetric analysis of FLAG-positive structures in retinal cross sections and isolated wholemounts was performed using Imaris software (Bitplane).

EM

Eyeballs were fixed via trans-cardial perfusion with 2% paraformaldehyde, 2% glutaraldehyde, and 0.05% calcium chloride in 50 mM MOPS, pH 7.4. Tissue processing was done according to a previously described procedure (Ding et al., 2015) as follows. Retinal vibratome sections were treated with 1% tannic acid (Electron Microscopy Sciences) and 1% uranyl acetate, dehydrated with graded ethanol, and infiltrated and embedded in Spurr's resin. For the developmental study in Fig. 3, eyeballs were fixed by immersion into a solution containing 2% paraformaldehyde and 2% glutaraldehyde in 0.1 M sodium cacodylate buffer. Eyeballs were then treated with 2% osmium tetroxide, dehydrated, and embedded. For experiments with cell culture, cells were fixed in a solution containing 2% paraformaldehyde and 2% glutaraldehyde in 0.1 M sodium cacodylate buffer, treated with 2% osmium tetroxide, dehydrated, and embedded in Spurr's resin. Thin sections of 60–80 nm were collected on copper grids, counterstained with uranyl acetate and Sato's lead, and examined using an electron microscope (JEM-1400; JEOL) at 60 kV. Images were collected using a charge-coupled device camera (Orius; Gatan). The Feret diameter, which is the maximum diameter of an ovoid object, was measured using ImageJ software (National Institutes of Health).

Postembedment immunogold

Tissue was processed according to the procedure described by Ding et al. (2015) as follows. Vibratome sections were treated with 0.5% tannic acid and cryoprotected with 30% glycerol in 0.1 M sodium acetate. Sections were freeze substituted overnight in 4% uranyl acetate/95% methanol at −78°C with gentle shaking on dry ice. Sections were rinsed with methanol, infiltrated with Lowicryl HM-20 (Electron Microscopy Sciences), slowly warmed to 0°C, and embedded for 3 d under ultraviolet light. Thin sections of 60–80 nm were cut and collected on nickel grids. Grids were treated with 10 mM citric buffer, pH 6.0, containing 0.005% Tergitol NP-10 for 15 min at 60°C, rinsed with water, blocked with 1% glycine in Tris-buffered saline, pH 7.6, containing 0.005% Tergitol NP-10 for 30 min, and incubated overnight with the primary antibodies 4D2 against rhodopsin (1:5,000) or rabbit polyclonal against FLAG (1:10,000). Grids were rinsed with buffer, blocked with 1% donkey serum, probed with donkey anti–mouse or anti–rabbit IgG conjugated to 12- or 18-nm colloidal gold particles (1:50; Jackson ImmunoResearch Laboratories, Inc.) for 2 h, rinsed, and counterstained with uranyl acetate and Sato's lead.

Immunofluorescence analysis in cell culture

AD293 cells were plated onto poly-L-lysine glass coverslips (354085; Corning) in a 24-well plate and grown overnight at 37°C. The next day, media were replaced with DMEM containing 2% FBS, and transfections were performed using Lipofectamine 3000 (L3000001; Invitrogen) according to the manufacturer's protocol. Cells were then grown for 2 d in the same medium at 37°C. Transfected cells were fixed in methanol for 5 min at −20°C, switched into 1:1 methanol/acetone for 5 min at −20°C, rinsed three times with PBS, and permeabilized for 10 min with 0.1% Triton X-100 in PBS, and nonspecific binding was blocked by a 1-h incubation in PBS containing 3% BSA. Coverslips were incubated overnight at 4°C with primary antibody diluted in blocking buffer, washed three times in PBS, and incubated for 2 h at 23°C with Hoechst and goat secondary antibodies conjugated with Alexa Fluor 488, 568, or 647. Coverslips were washed and mounted on slides with Immunomount (Thermo Fisher Scientific). Images were acquired using an Eclipse 90i microscope equipped with a 100× oil immersion objective (1.40 NA; Plan Apochromat VC) and an A1 confocal scanner controlled by NIS-Elements Advanced Research software for image acquisition.

Statistical analyses

Statistical analyses were performed using the two-tailed unpaired Student's *t* test for comparing two groups. The methods for statistical analysis and sample sizes are specified in either the Results or figure legends. Data distribution was proven to be normal in Fig. 1 B and assumed to be normal in other instances. Differences were accepted as significant for $P < 0.05$.

Online supplemental material

Fig. S1 shows the comparison of the outer segment/cilium length during postnatal development of rods in WT and *rds*$^{-/-}$ mice. Fig. S2 shows FLAG immunostaining in cross sections of WT retinas transfected with peripherin, Per-CT, Per-TS, and rhodopsin constructs. Fig. S3 shows FLAG immunogold labeling of a subretinal tubular membrane cluster in an *rds*$^{-/-}$ retina electroporated with Per-TS construct. Fig. S4 shows FLAG and Rom-1 immunostaining of retinal wholemounts from *rds*$^{-/-}$ mice transfected with peripherin, Per-CT, or Per-TS constructs. Fig. S5 shows FLAG immunostaining of retinal wholemounts from *rds*$^{-/-}$ mice transfected with two G protein–coupled receptor constructs fused to the peripherin C terminus.

Acknowledgments

This work was supported by the National Institutes of Health grants EY22862 (to R.Y. Salinas), EY025732 (to J.N. Pearring), EY025558 (to W.J. Spencer), EY12859 (to V.Y. Arshavsky), and EY5722 (to V.Y. Arshavsky) and the Research to Prevent Blindness Nelson Trust Award and unrestricted grant (to V.Y. Arshavsky).

The authors declare no competing financial interests.

Submitted: 23 August 2016
Revised: 22 December 2016
Accepted: 14 February 2017

References

Arshavsky, V.Y., and M.E. Burns. 2012. Photoreceptor signaling: supporting vision across a wide range of light intensities. *J. Biol. Chem.* 287:1620–1626. http://dx.doi.org/10.1074/jbc.R111.305243

Boesze-Battaglia, K., and A.F. Goldberg. 2002. Photoreceptor renewal: a role for peripherin/rds. *Int. Rev. Cytol.* 217:183–225. http://dx.doi.org/10.1016/S0074-7696(02)17015-X

Burgoyne, T., I.P. Meschede, J.J. Burden, M. Bailly, M.C. Seabra, and C.E. Futter. 2015. Rod disc renewal occurs by evagination of the ciliary plasma membrane that makes cadherin-based contacts with the inner segment. *Proc. Natl. Acad. Sci. USA.* 112:15922–15927. http://dx.doi.org/10.1073/pnas.1509285113

Cao, M., J. Ning, C.I. Hernandez-Lara, O. Belzile, Q. Wang, S.K. Dutcher, Y. Liu, and W.J. Snell. 2015. Uni-directional ciliary membrane protein trafficking by a cytoplasmic retrograde IFT motor and ciliary ectosome shedding. *eLife.* 4:e05242. http://dx.doi.org/10.7554/eLife.05242

Chuang, J.Z., Y. Zhao, and C.H. Sung. 2007. SARA-regulated vesicular targeting underlies formation of the light-sensing organelle in mammalian rods. *Cell.* 130:535–547. http://dx.doi.org/10.1016/j.cell.2007.06.030

Cocucci, E., and J. Meldolesi. 2011. Ectosomes. *Curr. Biol.* 21:R940–R941 (published correction appears in *Curr. Biol.* 2012. 22:1359). http://dx.doi.org/10.1016/j.cub.2011.10.011

Cohen, A.I. 1983. Some cytological and initial biochemical observations on photoreceptors in retinas of rds mice. *Invest. Ophthalmol. Vis. Sci.* 24:832–843.

Connell, G., R. Bascom, L. Molday, D. Reid, R.R. McInnes, and R.S. Molday. 1991. Photoreceptor peripherin is the normal product of the gene responsible for retinal degeneration in the rds mouse. *Proc. Natl. Acad. Sci. USA.* 88:723–726. http://dx.doi.org/10.1073/pnas.88.3.723

Ding, J.D., R.Y. Salinas, and V.Y. Arshavsky. 2015. Discs of mammalian rod photoreceptors form through the membrane evagination mechanism. *J. Cell Biol.* 211:495–502. http://dx.doi.org/10.1083/jcb.201508093

Geneva, I.I., H.Y. Tan, and P.D. Calvert. 2017. Untangling ciliary access and enrichment of two rhodopsin-like receptors using quantitative fluorescence microscopy reveals cell-specific sorting pathways. *Mol. Biol. Cell.* 28:554–566. http://dx.doi.org/10.1091/mbc.E16-07-0549

Goldberg, A.F.X., O.L. Moritz, and D.S. Williams. 2016. Molecular basis for photoreceptor outer segment architecture. *Prog. Retin. Eye Res.* 55:52–81. http://dx.doi.org/10.1016/j.preteyeres.2016.05.003

Gospe, S.M., S.A. Baker, and V.Y. Arshavsky. 2010. Facilitative glucose transporter Glut1 is actively excluded from rod outer segments. *J. Cell Sci.* 123:3639–3644. http://dx.doi.org/10.1242/jcs.072389

Han, Z., D.W. Anderson, and D.S. Papermaster. 2012. Prominin-1 localizes to the open rims of outer segment lamellae in *Xenopus laevis* rod and cone photoreceptors. *Invest. Ophthalmol. Vis. Sci.* 53:361–373. http://dx.doi.org/10.1167/iovs.11-8635

Händel, M., S. Schulz, A. Stanarius, M. Schreff, M. Erdtmann-Vourliotis, H. Schmidt, G. Wolf, and V. Höllt. 1999. Selective targeting of somatostatin receptor 3 to neuronal cilia. *Neuroscience.* 89:909–926. http://dx.doi.org/10.1016/S0306-4522(98)00354-6

Hogan, M.C., L. Manganelli, J.R. Woollard, A.I. Masyuk, T.V. Masyuk, R. Tammachote, B.Q. Huang, A.A. Leontovich, T.G. Beito, B.J. Madden, et al. 2009. Characterization of PKD protein-positive exosome-like vesicles. *J. Am. Soc. Nephrol.* 20:278–288. http://dx.doi.org/10.1681/ASN.2008060564

Huttner, W.B., and J. Zimmerberg. 2001. Implications of lipid microdomains for membrane curvature, budding and fission. *Curr. Opin. Cell Biol.* 13:478–484. http://dx.doi.org/10.1016/S0955-0674(00)00239-8

Iglič, A., H. Hägerstrand, P. Veranic, A. Plemenitas, and V. Kralj-Iglic. 2006. Curvature-induced accumulation of anisotropic membrane components and raft formation in cylindrical membrane protrusions. *J. Theor. Biol.* 240:368–373. http://dx.doi.org/10.1016/j.jtbi.2005.09.020

Jansen, H.G., and S. Sanyal. 1984. Development and degeneration of retina in rds mutant mice: electron microscopy. *J. Comp. Neurol.* 224:71–84. http://dx.doi.org/10.1002/cne.902240107

Kedzierski, W., J. Weng, and G.H. Travis. 1999. Analysis of the rds/peripherin·rom1 complex in transgenic photoreceptors that express a chimeric protein. *J. Biol. Chem.* 274:29181–29187. http://dx.doi.org/10.1074/jbc.274.41.29181

Keresztes, G., K.A. Martemyanov, C.M. Krispel, H. Mutai, P.J. Yoo, S.F. Maison, M.E. Burns, V.Y. Arshavsky, and S. Heller. 2004. Absence of the RGS9·Gβ5 GTPase-activating complex in photoreceptors of the R9AP knockout mouse. *J. Biol. Chem.* 279:1581–1584. http://dx.doi.org/10.1074/jbc.C300456200

Kevany, B.M., Y. Tsybovsky, I.D. Campuzano, P.D. Schnier, A. Engel, and K. Palczewski. 2013. Structural and functional analysis of the native peripherin-ROM1 complex isolated from photoreceptor cells. *J. Biol. Chem.* 288:36272–36284. http://dx.doi.org/10.1074/jbc.M113.520700

Khattree, N., L.M. Ritter, and A.F. Goldberg. 2013. Membrane curvature generation by a C-terminal amphipathic helix in peripherin-2/rds, a tetraspanin required for photoreceptor sensory cilium morphogenesis. *J. Cell Sci.* 126:4659–4670. http://dx.doi.org/10.1242/jcs.126888

Kinney, M.S., and S.K. Fisher. 1978. The photoreceptors and pigment epithelium of the larval Xenopus retina: morphogenesis and outer segment renewal. *Proc. R. Soc. Lond. B Biol. Sci.* 201:149–167. http://dx.doi.org/10.1098/rspb.1978.0037

Ma, J., J.C. Norton, A.C. Allen, J.B. Burns, K.W. Hasel, J.L. Burns, J.G. Sutcliffe, and G.H. Travis. 1995. *Retinal degeneration slow* (*rds*) in mouse results from simple insertion of a *t* haplotype-specific element into protein-coding exon II. *Genomics.* 28:212–219. http://dx.doi.org/10.1006/geno.1995.1133

Matsuda, T., and C.L. Cepko. 2004. Electroporation and RNA interference in the rodent retina in vivo and in vitro. *Proc. Natl. Acad. Sci. USA.* 101:16–22. http://dx.doi.org/10.1073/pnas.2235688100

Matsuda, T., and C.L. Cepko. 2007. Controlled expression of transgenes introduced by in vivo electroporation. *Proc. Natl. Acad. Sci. USA.* 104:1027–1032. http://dx.doi.org/10.1073/pnas.0610155104

Molday, R.S., D. Hicks, and L. Molday. 1987. Peripherin. A rim-specific membrane protein of rod outer segment discs. *Invest. Ophthalmol. Vis. Sci.* 28:50–61.

Nager, A.R., J.S. Goldstein, V. Herranz-Perez, D. Portran, F. Ye, J.M. Garcia-Verdugo, and M.V. Nachury. 2017. An actin network dispatches ciliary GPCRs into extracellular vesicles to modulate signaling. *Cell.* 168:252–263. http://dx.doi.org/10.1016/j.cell.2016.11.036

Nir, I., and D.S. Papermaster. 1986. Immunocytochemical localization of opsin in the inner segment and ciliary plasma membrane of photoreceptors in retinas of rds mutant mice. *Invest. Ophthalmol. Vis. Sci.* 27:836–840.

Nour, M., X.Q. Ding, H. Stricker, S.J. Fliesler, and M.I. Naash. 2004. Modulating expression of peripherin/*rds* in transgenic mice: critical levels and the effect of overexpression. Invest. Ophthalmol. Vis. Sci. 45:2514–2521. http://dx.doi.org/10.1167/iovs.04-0065

Pearring, J.N., R.Y. Salinas, S.A. Baker, and V.Y. Arshavsky. 2013. Protein sorting, targeting and trafficking in photoreceptor cells. Prog. Retin. Eye Res. 36:24–51. http://dx.doi.org/10.1016/j.preteyeres.2013.03.002

Pearring, J.N., E.C. Lieu, J.R. Winter, S.A. Baker, and V.Y. Arshavsky. 2014. R9AP targeting to rod outer segments is independent of rhodopsin and is guided by the SNARE homology domain. Mol. Biol. Cell. 25:2644–2649. http://dx.doi.org/10.1091/mbc.E14-02-0747

Pearring, J.N., W.J. Spencer, E.C. Lieu, and V.Y. Arshavsky. 2015. Guanylate cyclase 1 relies on rhodopsin for intracellular stability and ciliary trafficking. eLife. 4:e12058. http://dx.doi.org/10.7554/eLife.12058

Phua, S.C., S. Chiba, M. Suzuki, E. Su, E.C. Roberson, G.V. Pusapati, M. Setou, R. Rohatgi, J.F. Reiter, K. Ikegami, and T. Inoue. 2017. Dynamic remodeling of membrane composition drives cell cycle through primary cilia excision. Cell. 168:264–279. http://dx.doi.org/10.1016/j.cell.2016.12.032

Rattner, A., P.M. Smallwood, J. Williams, C. Cooke, A. Savchenko, A. Lyubarsky, E.N. Pugh, and J. Nathans. 2001. A photoreceptor-specific cadherin is essential for the structural integrity of the outer segment and for photoreceptor survival. Neuron. 32:775–786. http://dx.doi.org/10.1016/S0896-6273(01)00531-1

Rattner, A., J. Chen, and J. Nathans. 2004. Proteolytic shedding of the extracellular domain of photoreceptor cadherin. Implications for outer segment assembly. J. Biol. Chem. 279:42202–42210. http://dx.doi.org/10.1074/jbc.M407928200

Salinas, R.Y., S.A. Baker, S.M. Gospe III, and V.Y. Arshavsky. 2013. A single valine residue plays an essential role in peripherin/rds targeting to photoreceptor outer segments. PLoS One. 8:e54292. http://dx.doi.org/10.1371/journal.pone.0054292

Sanyal, S., and H.G. Jansen. 1981. Absence of receptor outer segments in the retina of *rds* mutant mice. Neurosci. Lett. 21:23–26. http://dx.doi.org/10.1016/0304-3940(81)90051-3

Sedmak, T., and U. Wolfrum. 2011. Intraflagellar transport proteins in ciliogenesis of photoreceptor cells. Biol. Cell. 103:449–466. http://dx.doi.org/10.1042/BC20110034

Sjöstrand, F.S. 1953. The ultrastructure of the outer segments of rods and cones of the eye as revealed by the electron microscope. J. Cell. Comp. Physiol. 42:15–44. http://dx.doi.org/10.1002/jcp.1030420103

Sorokin, S. 1962. Centrioles and the formation of rudimentary cilia by fibroblasts and smooth muscle cells. J. Cell Biol. 15:363–377. http://dx.doi.org/10.1083/jcb.15.2.363

Steinberg, R.H., S.K. Fisher, and D.H. Anderson. 1980. Disc morphogenesis in vertebrate photoreceptors. J. Comp. Neurol. 190:501–518. http://dx.doi.org/10.1002/cne.901900307

Stuck, M.W., S.M. Conley, and M.I. Naash. 2016. PRPH2/RDS and ROM-1: Historical context, current views and future considerations. *Prog. Retin. Eye Res.* 52:47–63. http://dx.doi.org/10.1016/j.preteyeres.2015.12.002

Tam, B.M., O.L. Moritz, L.B. Hurd, and D.S. Papermaster. 2000. Identification of an outer segment targeting signal in the Cooh terminus of rhodopsin using transgenic *Xenopus laevis*. *J. Cell Biol.* 151:1369–1380. http://dx.doi.org/10.1083/jcb.151.7.1369

Tam, B.M., O.L. Moritz, and D.S. Papermaster. 2004. The C terminus of peripherin/rds participates in rod outer segment targeting and alignment of disk incisures. *Mol. Biol. Cell.* 15:2027–2037. http://dx.doi.org/10.1091/mbc.E03-09-0650

Travis, G.H., M.B. Brennan, P.E. Danielson, C.A. Kozak, and J.G. Sutcliffe. 1989. Identification of a photoreceptor-specific mRNA encoded by the gene responsible for retinal degeneration slow (*rds*). *Nature.* 338:70–73. http://dx.doi.org/10.1038/338070a0

Usukura, J., and D. Bok. 1987. Changes in the localization and content of opsin during retinal development in the *rds* mutant mouse: immunocytochemistry and immunoassay. *Exp. Eye Res.* 45:501–515. http://dx.doi.org/10.1016/S0014-4835(87)80061-1

Volland, S., L.C. Hughes, C. Kong, B.L. Burgess, K.A. Linberg, G. Luna, Z.H. Zhou, S.K. Fisher, and D.S. Williams. 2015. Three-dimensional organization of nascent rod outer segment disk membranes. *Proc. Natl. Acad. Sci. USA.* 112:14870–14875. http://dx.doi.org/10.1073/pnas.1516309112

Wang, J., M. Silva, L.A. Haas, N.S. Morsci, K.C. Nguyen, D.H. Hall, and M.M. Barr. 2014. *C. elegans* ciliated sensory neurons release extracellular vesicles that function in animal communication. *Curr. Biol.* 24:519–525. http://dx.doi.org/10.1016/j.cub.2014.01.002

Wood, C.R., and J.L. Rosenbaum. 2015. Ciliary ectosomes: transmissions from the cell's antenna. *Trends Cell Biol.* 25:276–285. http://dx.doi.org/10.1016/j.tcb.2014.12.008

Wood, C.R., K. Huang, D.R. Diener, and J.L. Rosenbaum. 2013. The cilium secretes bioactive ectosomes. *Curr. Biol.* 23:906–911. http://dx.doi.org/10.1016/j.cub.2013.04.019

Yang, Z., Y. Chen, C. Lillo, J. Chien, Z. Yu, M. Michaelides, M. Klein, K.A. Howes, Y. Li, Y. Kaminoh, et al. 2008. Mutant prominin 1 found in patients with macular degeneration disrupts photoreceptor disk morphogenesis in mice. *J. Clin. Invest.* 118:2908–2916.

Young, R.W. 1967. The renewal of photoreceptor cell outer segments. *J. Cell Biol.* 33:61–72. http://dx.doi.org/10.1083/jcb.33.1.61

Zacchigna, S., H. Oh, M. Wilsch-Bräuninger, E. Missol-Kolka, J. Jászai, S. Jansen, N. Tanimoto, F. Tonagel, M. Seeliger, W.B. Huttner, et al. 2009. Loss of the cholesterol-binding protein prominin-1/CD133 causes disk dysmorphogenesis and photoreceptor degeneration. *J. Neurosci.* 29:2297–2308. http://dx.doi.org/10.1523/JNEUROSCI.2034-08.2009